ASCE

Two-Dimensional Finite-Element Simulation of Periodic Barriers

Hsuan Wen Huang[1]; Jiaji Wang, Ph.D.[2]; Chunfeng Zhao, Ph.D.[3]; and Y. L. Mo, Ph.D., F.ASCE[4]

Abstract: A novel kind of seismic isolation technique called "Periodic Barriers," which combines trench-type wave barriers and metamaterial, is introduced in this research. Metamaterial possesses a unique frequency-selective property that enables the metamaterial to manipulate the wave propagation. By infilling the metamaterials in the trench-type wave barriers, the periodic barriers are expected to display advantages of both the wave barriers and the metamaterials. The two-dimensional (2D) finite-element (FE) simulation is conducted to study the performance of the barriers adapting the metamaterial. This FE model is validated with the experiment on the metamaterial-based foundation. The convergence test on mesh size with different element types are investigated, and the minimum mesh size and property element type are determined for simulating the behavior of metamaterial. To simulate the unbounded domain, the absorbing boundary is implemented to eliminate the reflection from the boundaries. The dynamic responses obtained from models with infinite element boundary and viscoelastic boundary are found to converge with the increasing model size. To boost the computing efficiency, two analysis methods (fix-frequency harmonic analysis, and the time-history analysis) are adopted and found to have a strong correlation with each other. Based on the proposed modeling techniques and the analysis methods, the simulation of the periodic barriers embedded in the soil is performed. With various loading distance and the number of periodic barriers, the performance of the periodic barriers is found to comply with its theoretical frequency band gaps. **DOI: 10.1061/(ASCE)EM.1943-7889.0001891.**

Author keywords: Metamaterial; Frequency band gap; Periodic barriers; Infinite boundary; Viscoelastic boundary; Finite-element (FE) simulation.

Introduction

When an earthquake occurs, the seismic waves travel from the source to the surface of the earth, carrying the energy released from the rupture along the fault. When the waves reach the ground surface, the subsequent shaking can bring devastating destruction to human civilization. In order to mitigate the seismic damage, many countermeasures, such as base isolations or dampers, have been proposed and practically implemented for decades in the earthquake-resistance design of the structures. The traditional seismic base isolation systems extend the natural period of the structures, while the traditional dampers add damping to the structures. On the other hand, the isolation of the metamaterial-based periodic barriers presented in this research is attributed to the inherent properties, i.e., frequency band gaps. These artificial materials are formed by periodically repeating cells. Based on the theory of periodic metamaterial, the propagation of elastic waves with frequencies within the frequency band gaps will be prohibited. Therefore, the metamaterial-based periodic barriers may notably reduce the seismic response of engineering structures. In addition, the periodic barriers are more feasible for construction in existing buildings compared to traditional base isolation systems and dampers. To propose a new type of seismic isolation, two key elements are involved in this research: wave barriers and metamaterials. First, the wave barriers originated from the idea of obstructing the man-made surface waves that attenuate the ground vibration by creating a discontinuity in the soil. In this research, the wave barriers are expected to attenuate the seismic waves with lower frequency content relative to man-made waves. Second, the metamaterials, developed in the branch of solid-state physics, possess a unique capability to manipulate the waves. Due to the interaction between the waves and its constituent materials, the metamaterial allows the propagation of elastic waves in some frequency ranges (frequency passband) and forbids the propagation in other frequency ranges (frequency band gap). The previous experimental and numerical studies had proven that the vibrations could be significantly mitigated by implementing the metamaterial in the form of a structural foundation. By infilling the metamaterials in the trench-type wave barrier, the periodic barriers are expected to display advantages of both the wave barriers and the metamaterials. Traditionally, the research in solid-state physics has shown that the metamaterials (also referred to as phononic crystals) can be used to manipulate the waves. The metamaterial can be engineered to forbid the vibration in the designed frequency band gap. This study aims to investigate if metamaterial can be an alternative as the infilled material of the trench-type wave barrier. The frequency selective property of the metamaterial allows the anticipation of the attenuation in certain frequency ranges.

[1]Master and Ph.D. Candidate, Dept. of Civil and Environmental Engineering, Univ. of Houston, Houston, TX 77204-4003. ORCID: https://orcid.org/0000-0001-7509-277X. Email: hhuang15@uh.edu

[2]Postdoctoral Associate, Dept. of Civil and Environmental Engineering, Univ. of Houston, Houston, TX 77204 (corresponding author). ORCID: https://orcid.org/0000-0002-6728-2685. Email: jwang215@central.uh.edu; wangjiaji.thu@gmail.com

[3]Associate Professor, Dept. of Civil Engineering, Hefei Univ. of Technology, Hefei, Anhui 230011. Email: zhaowindy@hfut.edu.cn

[4]John and Rebecca Moores Professor, Dept. of Civil and Environmental Engineering, Univ. of Houston, Houston, TX 77204-4003. Email: yilungmo@central.uh.edu

Note. This manuscript was submitted on June 15, 2020; approved on October 5, 2020; published online on December 7, 2020. Discussion period open until May 7, 2021; separate discussions must be submitted for individual papers. This paper is part of the ***Journal of Engineering Mechanics***, © ASCE, ISSN 0733-9399.

Wave Barrier

The wave barrier is a typical measure to isolate the vibration transmitted through the surface to reduce the undesired vibrations and has been studied numerically and experimentally. The wave barriers were developed for mitigating the vibration transmitted on the surface to the protected structure by introducing the discontinuity on the path of wave propagation. The wave barriers can be in various forms, such as open or infilled trench-type (Al-Hussaini and Ahmad 1991; Alzawi and El Naggar 2011; Çelebi et al. 2009) wave barrier and rows of piles (Gao et al. 2006; Kattis et al. 1999; Liao and Sangrey 1978). The typical form of wave barrier is the open trench or infilled trench wave barrier. Depending on the distance between the wave barriers and the vibration source, the wave barriers are classified into active and passive barriers. For the barriers installed near the vibration source, the wave barriers are classified into the active isolation (Gao et al. 2015; Wang et al. 2009), which is usually used when the location of the vibration source is known. For barriers installed close to the protected structures from the incoming wave, the wave barriers are classified into the passive isolation (Gao et al. 2006; Liao and Sangrey 1978).

Geometric limitations of the trench-type wave barriers such as barrier length and barrier depth show a notable effect on the screening effectiveness of the wave barriers. Woods (1968) conducted experiments to investigate the performance of the trench barrier under the vertical excitation and proposed design recommendations for the open trench barrier. Waas (1972) and Segol et al. (1978) used the frequency-domain two-dimensional (2D) finite-element (FE) model to study the behavior of open or infilled trenches and investigated the influence of medium material. Segol et al. (1978) reported that the normalized depth has to be higher than 0.6 for significant response reduction and agreed with Wood's assumption that the effect of barrier width is insignificant. In terms of the infilled material, the stiff barriers and the soft barriers were studied. When the Elastic modulus of the infilled material is larger than soil, this infilled wave barrier is called stiff barrier; when the Elastic modulus of the infilled material is smaller than soil, this infilled wave barrier is called soft barrier. Persson et al. (2016) conducted 2D FE analysis to conduct low-frequency traffic excitation on the soft barrier, and find out the soft filling material enhances the mitigation performance of a barrier. Saikia (2014) investigated the effect of the number of barriers filled with soft material and concluded the shear wave velocity ratio (which is defined by dividing the shear wave velocity of the barrier by the shear wave velocity of soil) within 0.1 to 0.15 has the optimized screening efficiency. Furthermore, three-dimensional (3D) FE simulations were reported (Ekanayake et al. 2014) to compare the performance of the open trench barrier and geofoam-infilled wave barrier to attenuating the ground vibration. The results of the geofoam-infilled trench are first validated by the full-scale field experiment (Alzawi and El Naggar 2011). Different infilled materials were later simulated to compare the efficiency of the wave barrier. Qiu (2014) conducted both 2D and 3D FE simulations to study the behavior of the underground structure under the vibration and reported that reducing the shear velocity of the barrier material increase the vibration mitigation performance of the wave barrier. From the 3D FE simulations, it was observed the response amplifies in front of the wave barrier. Alzawi and El Naggar (2011) and Coulier et al. (2015) conducted full-scale experiments and developed FE models to investigate the performance of the trench type wave barrier for blocking the vibration generated from the surface. The FE simulation result fits the field test result with adequate accuracy that proves the stiff wave barriers can result in remarkable vibration reduction.

Other than the traditional FE model, the boundary element model (BEM) was adopted to investigate the screening effectiveness of the wave barriers (Leung et al. 1990) with the soil simulated to be a viscoelastic half-space. Al-Hussaini and Ahmad (1991) investigated high-frequency surface waves with a parametric study and reported the effect of geometric and material properties on the performance of the infilled trench wave barrier. A simple design formula was proposed for the rectangular wave barrier under the horizontal excitation as a result. FE-BE models couple FE and BE in the same model. Using FE to simulate the track and BE to model the soil and infilled trench, FE-BE models are employed to analyze open and soft infilled trench barriers (Thompson et al. 2016) and the influence of excitation direction (Andersen and Nielsen 2005) from the track. The results show that the depth of the wave barrier is recommended to be more than 60% of the Rayleigh wavelength of soil, and the efficiency of the infilled material is strongly affected by the exciting frequency and excitation direction.

Metamaterial-Based Isolation System

The importance of the infilled material was identified in the previous study. The proposed periodic barrier is the trench-type wave barrier infilled with metamaterial. The concept of metamaterials, originating from solid-state physics, is the composite material arranged periodically that can display a unique frequency-selective property. When the exciting frequency lies within a certain frequency range (frequency band gap), the wave propagation will be prohibited. The metamaterial is categorized into one-dimensional (1D), 2D, and 3D. Shi et al. (Bao et al. 2011; Cheng and Shi 2013; Huang and Shi 2013; Jia and Shi 2010) carried out several studies regarding the 1D or 2D metamaterial for earthquake isolation. Experiments adopting the metamaterial to the base isolation system called periodic foundation were also reported (Witarto et al. 2018, 2019; Xiang et al. 2012; Yan et al. 2014a, b, 2015). The test results showed that a significant reduction could be achieved by the implemented periodic foundation as the base isolation system. Many researchers have explored the trench-type wave barrier from the perspective of the metamaterial by treating the soil as part of the metamaterial (Pu and Shi 2019). However, because the soil is highly inhomogeneous at the real site, the material properties of the soil are hard to be determined when designing the metamaterial. For actual practice, authors would also suggest excluding the soil as part of the metamaterial and only focusing on the part that is well controlled. Therefore, in this study, the soil is excluded in calculating the theoretical frequency band gaps of the periodic barrier.

For periodic barriers buried in soil, many researchers have validated the accuracy of the 2D FE model with plane strain assumption by experimental study and 3D FE models. For example, Huang and Shi (2013) conducted the 2D FE simulation on the 2D infinite periodic pile barrier subjected to plane waves, and it showed the screening effectiveness could be well predicted by the 2D FE models. Liu et al. (2015) compared the 2D FE models and 3D FE models for numerical simulation of vibration reduction by periodic pile barriers. As the pile length increases, the FRF in the 3D FE models converges to that in the 2D model. Thus, the 2D FE models can be used to study the dynamic response of periodic pile barriers with a sufficiently large pile length. Contrary to the common infilled material, using the metamaterial as the infilled material allows the anticipation of the response attenuation in the desired frequency ranges. In addition, due to its simplicity and low computation cost, the 2D FE simulation has been widely adopted for engineering design practice. Therefore, the 2D FE simulation is investigated in this research.

Although significant research has been conducted on the mesh size, boundary conditions, and external load on simulation of soil and superstructures, there is a dearth of systematic research on FE modeling scheme for the periodic barrier in the soil. The lack of such a modeling scheme has significantly restricted the application of the periodic barrier in the civil engineering community. In response to this issue, the modeling scheme for simulating the periodic barrier buried in the soil is carefully investigated in this research. The periodic barrier in the present paper adopts the concept of infilled trench-type wave barrier and 1D metamaterial consisted of concrete and rubber. First, the theoretical frequency band gap of the metamaterial is briefly illustrated. Subsequently, the seismic behavior of the metamaterial buried in the soil is investigated based on the FE model. The modeling scheme of the FE model is reported in detail, including the choice of element type and mesh size, the boundary condition, the simulation region size, and the choice loading method. The accuracy of the proposed FE model is first validated by a benchmark test (Witarto et al. 2018). In addition, the developed FE model is adopted to simulate the periodic barrier buried in the soil. The influence of key parameters is reported in detail. The convergence tests on the FE model size and the size of infinite boundary elements are studied, and the results are used to determine the minimum modeling region size and maximum mesh size for high-efficiency FE simulation. The screening efficiency of the periodic barrier is presented in the frequency domain. Finally, the parameters for analyzing the screening effectiveness of periodic barriers such as loading directions, loading distances, and the number of unit cells are investigated. The numerical results exhibit the existence of the frequency band gap and the effect of the surrounding soil on the performance of the periodic barrier.

Theoretical Frequency Band Gap of Periodic Barrier

Fig. 1 is a schematic drawing of a 1D metamaterial with an infinite number of 3-layer unit cells. Each layer in a unit cell has different material properties including Young's modulus, Poisson ratio, and mass density. This section briefly illustrates the theory of the frequency band gap.

Eq. (1) is the governing equation of wave propagating in solid

$$\frac{\partial^2 \mathbf{u}}{\partial t^2} = \frac{1}{\rho}\{\nabla(\lambda + 2\mu)\nabla \cdot \mathbf{u} - \nabla \times (\mu \nabla \times \mathbf{u})\} \tag{1}$$

where $\mathbf{u}$ = displacement vector; λ and μ = Lame constants; ρ = density; and t = time.

The theory begins with the assumption that the wave propagates in metamaterial with an infinite number of unit cells periodically arranged. Bloch's theorem introduces a way to express the wave propagates in the periodic structure. It decomposes the solution to periodic function and phase term. The periodic function part shares the same periodicity of the periodic structure, and the phase term contains the wave vector, which indicates the wave direction with the amplitude reciprocal to wavelength. By putting this form of the solution in the original governing equation, the problem yields an eigenvalue problem. In this eigenvalue problem, every wave vector corresponds to an infinite number of eigenfrequencies. For a 1D metamaterial, $w(x, t)$ is the solution of the wave propagation satisfying the governing equation that can be expressed as

$$\mathbf{w}(x, t) = \hat{\mathbf{w}}(x, t)e^{ikx} \tag{2}$$

where $\hat{\mathbf{w}}(x, t)$ = periodic function.

When the metamaterial has the periodicity of a, the periodic function satisfies

$$\hat{\mathbf{w}}(x, t) = \hat{\mathbf{w}}(x + a, t) \tag{3}$$

Therefore, the periodicity is formulated as follows:

$$\mathbf{w}(x + a, t) = \hat{\mathbf{w}}(x + a, t)e^{ik(x+a)} = \hat{\mathbf{w}}(x, t)e^{ik(x+a)} = \mathbf{w}(x, t)e^{ika} \tag{4}$$

After solving the eigenvalue problem, the frequencies for each wavenumber k can be obtained. The wavenumber and its eigenfrequencies form the dispersion relationship that shows the wave characteristics in metamaterial including the frequency band gaps. The full derivation of the dispersion relationship can be found in the paper by Witarto et al. (2018).

The periodic barrier in this study is made of 3-layer unit cells of a 1D metamaterial. This layered metamaterial is illustrated in Fig. 2. The material properties of these three layers are as follows:

The first layer (concrete): $E_1 = 30.44$ GPa, $\rho_1 = 2{,}400$ kg/m^3, $\nu_1 = 0.2$, $h_1 = 101.6$ mm

The second layer (rubber): $E_2 = 0.1586$ MPa, $\rho_2 = 1{,}100$ kg/m^3, $\nu_2 = 0.463$, $h_2 = 76.2$ mm

The third layer (concrete): $E_3 = 30.44$ GPa, $\rho_3 = 2{,}400$ kg/m^3, $\nu_3 = 0.2$, $h_3 = 101.6$ mm

These three layers include two layers of concrete and one layer of rubber. Fig. 3 shows the resulting dispersion relation of the periodic barrier. The dispersion curve relates the frequency to the corresponding real wave number. The frequency band gap of the metamaterial can be identified in the dispersion relation that where the corresponding wavenumber is in complex form. When the exciting frequency lays within frequency band gaps, the wave propagation will be prohibited.

The resulting theoretical frequency band gaps within the range from 0 to 100 Hz for the unit cell are as follows. For the primary wave (P wave), the theoretical frequency is 45.0–100 Hz; for the shear wave (S wave), the theoretical frequency band gaps

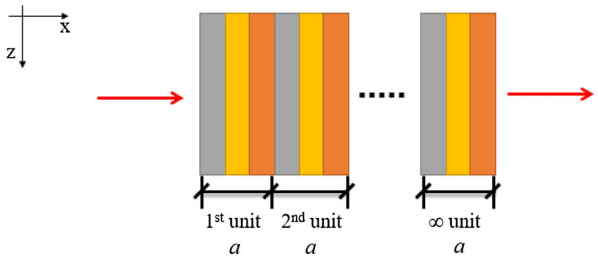

Fig. 1. 1D metamaterial with an infinite number of three-layer unit cells.

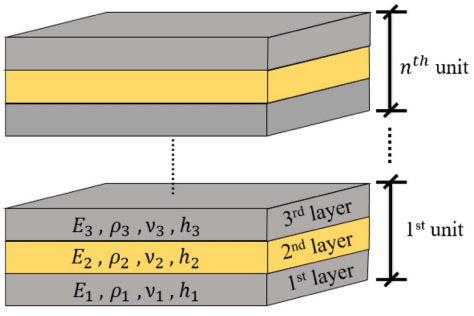

Fig. 2. Illustration of 1D periodic barrier.

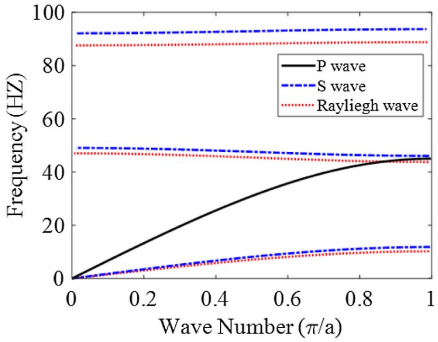

Fig. 3. Dispersion relation of periodic barrier.

are 11.8–46.1 Hz, 49.1–92.1 Hz, and 93.7–100 Hz; and for the Rayleigh wave, the band gaps are 10.2–43.8 Hz, 47.0–87.6 Hz, and 88.8–100 Hz.

Finite-Element Modeling Scheme

In this section, the commercial FE software ABAQUS version 6.14 is used to conduct 2D simulations for the performance of the 1D periodic barriers under seismic load and vibration. In this section, the following five key factors are illustrated in detail, including the element type, the mesh size, the boundary condition, the simulation region, and the analysis method.

Element Type and Mesh Size

The element type and mesh size significantly influence the FE simulation result. In this research, the 2D simulation is adopted with plane strain assumption (Al-Hussaini and Ahmad 1991; Alzawi and El Naggar 2011; Beskos et al. 1986; Persson et al. 2016; Qiu 2014; Saikia 2014), which assumes the barrier is infinitely long. The linear element (CPE4R) and the quadratic element (CPE8R) with reduced integration are adopted for FE simulation. The convergence tests are conducted for different mesh sizes using different element types, and the accuracy is verified with the theoretical frequency band gaps. This convergence test should help identify the appropriate mesh type and mesh size that can accurately capture the behavior of the periodic barriers.

Infinite Element and Viscous-Elastic Element

The absorbing boundaries are deployed to simulate the unbounded domain. In this research, the infinite boundary and viscoelastic boundary are adopted, as shown in Figs. 4(a and b), respectively.

For the infinite boundary, the four-node linear, one-way infinite element with plane strain assumption (CINPE4) is used for the plane strain condition. The infinite element reduces the reflection of vibration energy by suppressing the stiffness and adding damping on the boundary (Smith 2016). The infinite boundary provides the perfect transmission of energy when the wave incidence is orthogonal to the boundary. Even though the infinite element cannot provide the perfect absorption when the incident wave is not perpendicular to the boundary, it still absorbs energy and provides an acceptable result for practical cases. For the viscoelastic boundary element, as shown in Fig. 4(b), the parallel system consists of stiffness and damping in both tangent and normal directions at the boundary. According to Shi et al. (2017), for a 2D problem, the normal and tangent stiffness and damping are obtained as follows:

$$k_n = \alpha_n \frac{\mu}{r_d} \tag{5}$$

$$c_n = \rho C_P \tag{6}$$

$$k_r = \alpha_\tau \frac{\mu}{r_d} \tag{7}$$

$$c_r = \rho C_S \tag{8}$$

where k_n = normal stiffness; c_n = normal damping; k_r = tangential stiffness; c_r = tangential damping; α_n = coefficient ranging from 0.8 to 1.2; and α_τ = coefficient ranging from 0.35 to 0.65. In this research, the average values of 1.0 and 0.5 are selected for α_n and α_τ, respectively: μ = shear modulus; r_d = radius of the model; C_P = P wave velocity; and C_S = S wave velocity.

Because the infinite boundary element is the built-in element available in the FE software package, ABAQUS, it is fairly easy to implement while building the FE model on ABAQUS. However, its computing efficiency is rather low comparing to the viscoelastic boundary. On the other hand, the viscoelastic boundary is widely used, and its accuracy is verified by many researchers (Shi et al. 2017). However, the normal and tangent stiffness and damping deployed on the boundaries vary with different material properties, model region size, mesh size, and other coefficients. Therefore, implementing viscoelastic boundaries requires slightly more skills for the user compared to implementing infinite boundaries.

Simulation Region Size

The infinite boundary elements can reduce the reflection from the boundary. However, the one-way infinite element in ABAQUS cannot absorb the energy perfectly when the incident angle, defined by

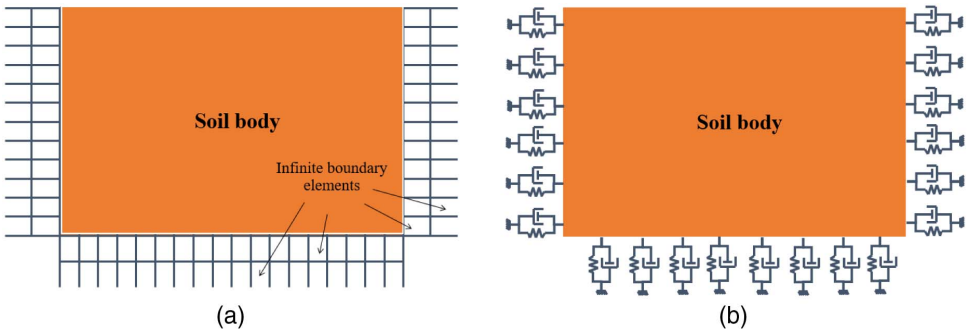

Fig. 4. Illustration of absorbing boundaries: (a) infinite boundary; and (b) viscoelastic boundary.

J. Eng. Mech., 2021, 147(2): 04020150

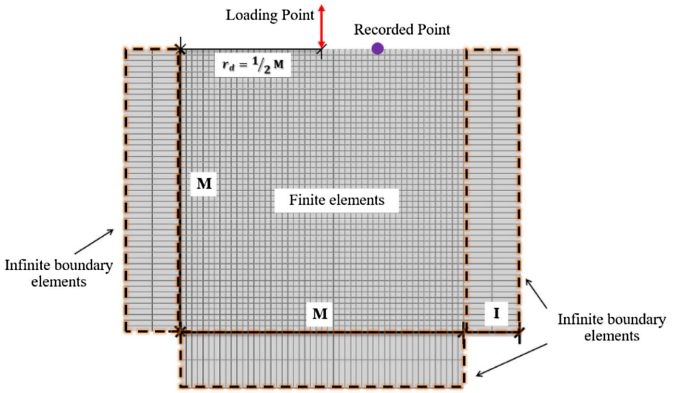

Fig. 5. Finite-element model with infinite boundary.

the direction of the wave front and normal direction of the boundary, is not 0. If the FE simulation region is extended, the induced reflection can be further reduced since the incident angle is reduced. To study the influence of the model size (denoted as M) and the thickness of the infinite elements (denoted as I), the model made of homogenous soil material is built as shown in Fig. 5. The infinite boundaries are implemented on the left, right, and bottom edges of the model to simulate the unbound domain. The loading point is placed around the center of the FE simulation region, and the response is recorded 0.5 m away from the loading point.

In this research, I/M ratios ranging from 0.05 to 1 for M equals to 5, 10, and 50 m are tested to study the effect of the model size and size of infinite boundary elements. The 30-Hz harmonic excitation is applied at the loading point in the vertical direction with an amplitude of 0.01 g.

Frequency Response Function

The isolation performance of the periodic barriers is defined by frequency response function, FRF, which is derived from the average reduction factor (RF). RF is a typical measure to evaluate the performance of the wave barriers by comparing the response of the soil surface in the presence of the wave barrier (A_w) with the response without the wave barrier (A_n) in the direction of excitation

$$RF = \frac{A_w}{A_n} \tag{9}$$

In this research, the total screening effectiveness is evaluated by the average reduction factor $\overline{RF}$, which is the average over a certain distance from the edge of the barrier. The wave barrier is expected to reduce the soil particle response in an area behind the wave barrier. The lower value of the average reduction factor indicates that the barrier is more effective. It is a common practice to calculate the performance of the wave barrier over a certain extent behind the barrier (Al-Hussaini and Ahmad 1991; Huang et al. 2017). By averaging over a certain extent, the error caused by local effects can be eliminated. The average amplitude reduction factor is calculated as follows:

$$\overline{RF} = \frac{1}{L}\int_0^L RF\,dx \tag{10}$$

where L = distance affected by the vibration. In this research, L is fixed at 3 times a Rayleigh wave wavelength (λ_R).

A typical way to express the attenuation of the metamaterial is the FRF as follows:

$$FRF = 20\log(\overline{RF}) \tag{11}$$

where negative FRF shows reduced responses, while positive FRF shows amplified responses.

Fix-Frequency Harmonic Analysis and Time-History Analysis

Two analysis methods are used in this study. One is termed fix-frequency harmonic analysis, and the other is time-history analysis. The differences between these two analysis methods are their loading protocol and the way to process data.

For fix-frequency harmonic analysis, the continuous sine wave with fixed frequency is used as the loading protocol. The frequencies considered in fix-frequency harmonic analysis are ranging from 15 to 100 Hz with a 5-Hz interval. The RF at each point behind the periodic barrier can be evaluated by comparing those maximum responses with barriers and the maximum responses without barriers for each exciting frequency. For time-history analysis, the earthquake's seismogram is used as the loading protocol. After transforming the response from the time domain into the frequency domain for cases with and without the periodic barrier, the average reduction factor can be obtained for each point at all frequencies. For both analysis method, the FRF will be obtained by the average reduction factor within the measuring extent, $3\lambda_R$. The FRF results obtained from the time-history analysis are smoothed using the built-in function, SMOOTH, in Matlab version 2015b with local regression using weighted linear least squares and a 2nd-degree polynomial model. The advantage of using time-history analysis is that it can reduce computing time and still maintain acceptable accuracy. For both methods, the requirement for the maximum time increment Δt is set to be $1/(10f_{max})$. Because the frequency of interest in this study is between 15 and 100 Hz, the maximum time increment is set to 0.001 s in the FE models.

Validation and Verification of FE Model

Benchmark Problem

A shake table test was conducted by Witarto et al. (2018) to study the seismic isolation performance of the large-scale 1D metamaterial-based foundation, i.e., periodic foundation. The experimental setup and the specimen detail can be found in Witarto et al. (2018). The first and second theoretical frequency band gaps of the periodic foundation subjected to S wave are found to be 18.1–20.4 Hz and 28.9–50 Hz, respectively. The frequency sweeping test was adopted to verify the accuracy of the developed FE model in predicting the frequency band gap of the periodic foundation. In the frequency sweeping test, the input wave was a continuous series of sine waves starting from 1 to 50 Hz. The S wave is generated by shaking the table in the horizontal direction. Fig. 6 shows the horizontal acceleration input from the shake table, and the horizontal output recorded acceleration on the top surface of the periodic foundation for frequency sweeping test. The shake table input is marked in black, and the output is recorded on top of the periodic foundation marked as red. Using Fast Fourier Transform (FFT), the input and output are converted to the frequency domain and shown in Fig. 7.

Validation and Verification Based on a Benchmark Problem

To validate the FE modeling scheme, the test results for the periodic foundation is simulated using the FE analysis. There are two parts

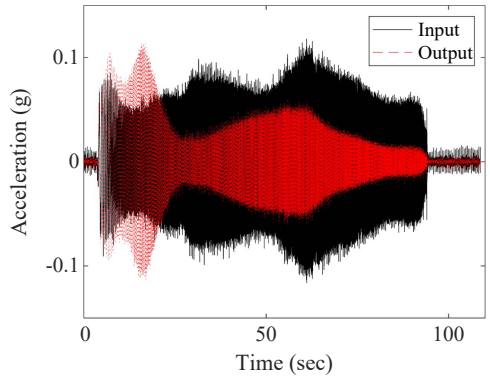

Fig. 6. Frequency sweeping test results of periodic foundation in the horizontal direction.

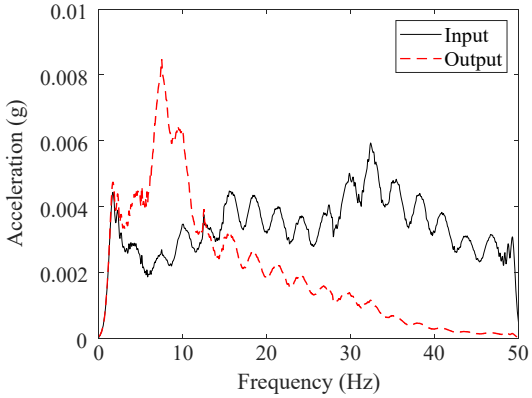

Fig. 7. Fourier spectra of frequency sweeping test results of periodic foundation in the horizontal direction.

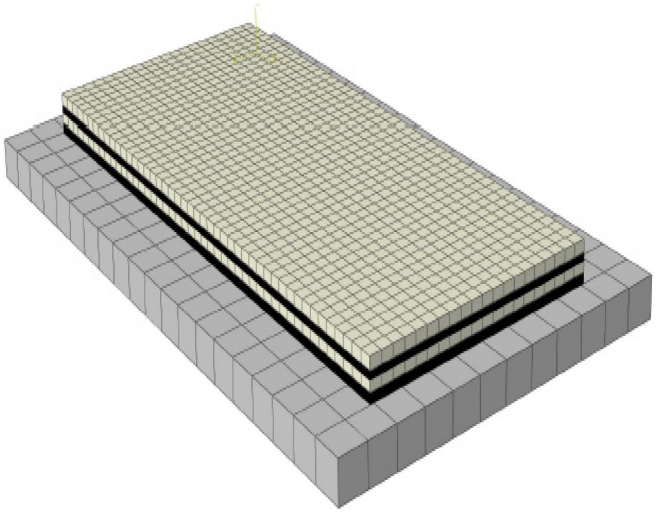

Fig. 8. FE model of the 1D periodic foundation.

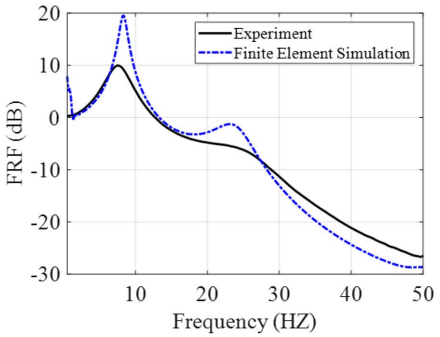

Fig. 9. Experimental and simulation results.

to validate: one is the FE modeling techniques, and the other is the analysis method, i.e., time-history analysis. The quadratic elements are used for the rubber layer of the periodic foundation. The rubber layer is meshed into two layers to better depict the dynamic behavior of the rubber material. An earthquake, El Centro, is applied on the bottom of the periodic foundation to simulate the motion of the shake table. It is worth noting that the input signal used in the simulation is different from the input signal used in the shake table test for the reason to test if the time-history analysis method is valid. The results of input and output are converted to the frequency domain. The resulting *FRF* is obtained by comparing the recorded output and input in the frequency domain.

Fig. 8 shows the FE model of the 1D periodic foundation in ABAQUS. Shown in Fig. 9, the simulation result agrees with the experimental result and the theoretical frequency band gaps. This has proven the FE modeling techniques are valid. Moreover, it shows that even with a different input signal, the time-history analysis can yield a certain degree of accuracy.

Influence of Key Parameters

Influence of Element Type and Mesh Size Sensitivity

Fig. 10 shows the frequency sweeping analysis of a periodic barrier subjected to P wave and S wave to investigate the influence of element type and mesh size. The periodic barrier is modeled with the material properties listed previously. The P wave is simulated by harmonic vertical displacement excitation, while the S wave is simulated by harmonic horizontal displacement input. The output is recorded on top of the barrier. *FRF* is obtained by comparing displacement from the displacement input and output. The mesh size is primarily dominated by the smallest S wave wavelength and is further meshed along the thickness direction for a better simulation result. The concrete layer is denoted by C and the rubber layer is denoted by R, and each layer is cut into several layers. For example, when the concrete layer is meshed by two layers of elements, and the rubber layer is meshed by three layers of elements, the case is named C2R3. In addition to the mesh size, both linear elements and quadratic elements are used to investigate the effect of different mesh types. By increasing the order of the element, the FE simulation error should be reduced while resulting in more integration points and increased computing time. The FE results are plotted together with the theoretical frequency band gap in Figs. 11 and 12.

With the theoretical frequency band gap highlighted with yellow patches in the back, the *FRF* results are shown for each mesh size with either linear in Fig. 11 or quadratic elements in Fig. 12. With decreasing mesh size, the FE results are approaching the theoretical frequency band gap. However, with linear elements, it required more elements to better capture the responses; with quadratic elements, the response matches the theory for the mesh of C1R2. In addition, it is worth noting that there is a significant spike or amplification at a frequency of 35 Hz in the S wave results, even though the frequency is within the frequency band gaps. The spikes observed within the range of frequency band gap may be attributed

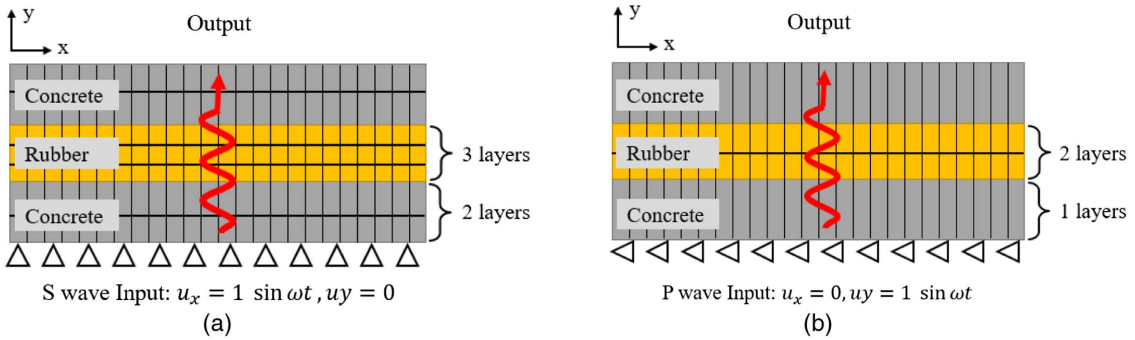

Fig. 10. Frequency sweeping test of periodic barrier (not to scale): (a) S wave for C2R3 mesh; and (b) P wave for C1R2.

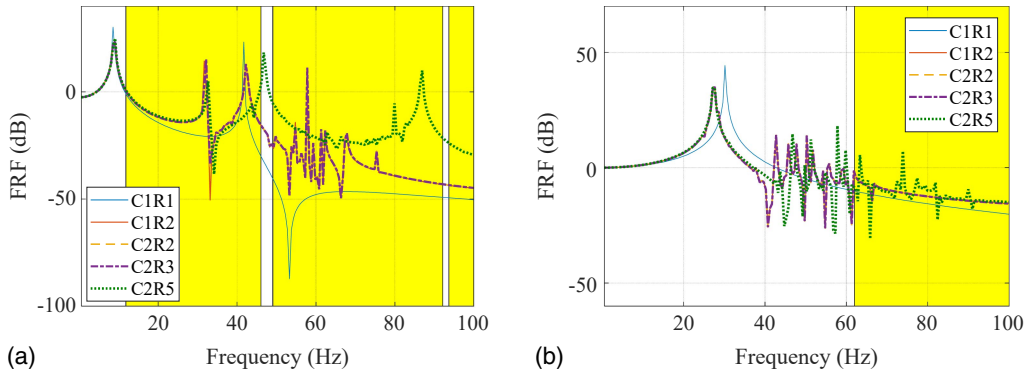

Fig. 11. *FRF* of FE models with linear elements: (a) S wave; and (b) P wave.

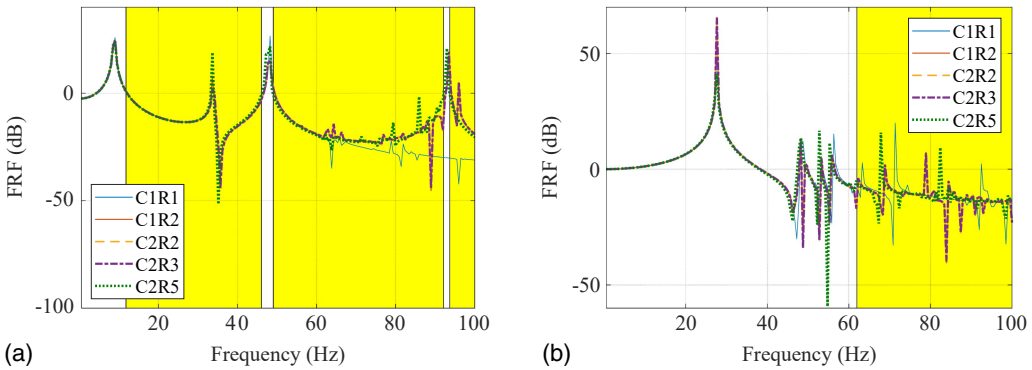

Fig. 12. *FRF* of FE models with quadratic elements: (a) S wave; and (b) P wave.

to the rocking mode produced by the model, which was not included in the theoretical derivation.

The quadratic element with at least two elements in the thickness direction of the rubber layer is recommended for simulating the dynamic behavior of the rubber material. Therefore, the mesh size of the rubber layer in the periodic barrier is set to 0.0038 m. The number of elements in the concrete layer has little influence on the results, so as few as one element in the thickness direction is adapted while simulating the periodic barrier.

Boundaries for Unbounded Domain

The following soil properties are used in this research: Young's modulus of 20 MPa, the density of 200 kg/m^3, and the Poisson ratio of 0.25. The derived parameters are Shear modulus μ of 8 MPa, the S wave speed of 200 m/s, and the P wave speed of 364.4 m/s. In order to investigate the performance of the infinite boundary and viscoelastic boundary, the FE model of homogenous soil material is built. The acceleration load is applied near the center of the FE region enclosed by the infinite boundary elements with 0.01 g amplitude. The size of the infinite boundary element is discussed along with the model size. The FE model meshes with linear plane strain elements with enhanced hourglass control. The mesh size is 0.1 m, which satisfies the requirement that the mesh size should be less than 1/8 minimum S wave wavelength with the given soil conditions.

Influence of the Thickness of inflnite Boundary Element

For infinite boundary elements, the 4-node linear, one-way infinite element with plane strain assumption (CINPE4) is used for the

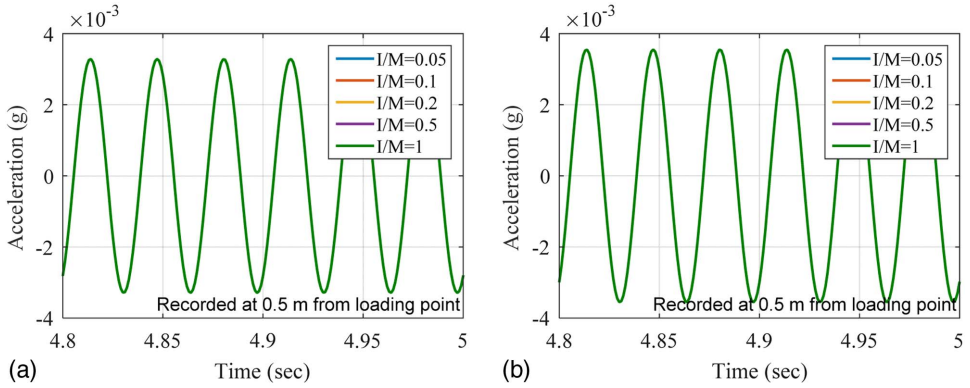

Fig. 13. Dynamic response under 30-Hz harmonic excitation: (a) model size of 5 m with infinite boundary; and (b) model size of 10 m with infinite boundary.

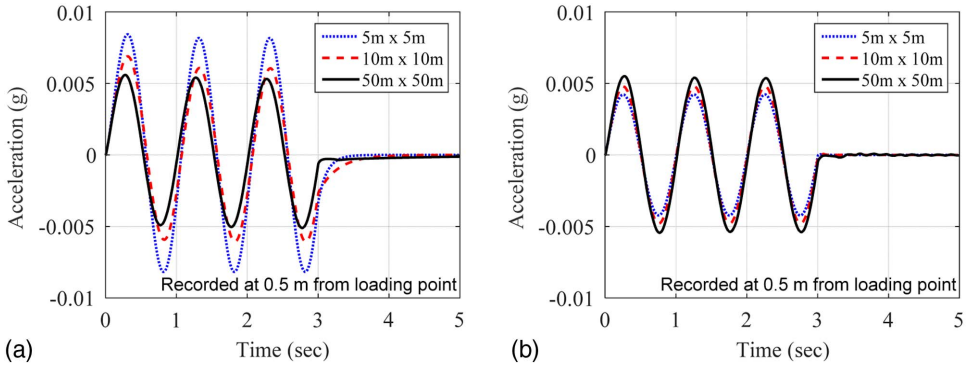

Fig. 14. Dynamic response under 4.77-Hz impulse excitation: (a) infinite boundary; and (b) viscoelastic boundary.

plane strain condition in the study. The effect of the *I*/*M* ratio is first investigated. In the parametric analysis, the model size (*M*), defined by the size of region modeled with finite elements, varied from 5 to 10 m, and the *I*/*M* ratio varied from 0.05 to 1 to investigate the effect of the model size and size of infinite boundary elements. The 30-Hz harmonic excitation is applied at the loading point in the vertical direction. Fig. 13 shows the response recorded 0.5 m away from the loading point with various model sizes and *I*/*M* ratios.

As shown in Fig. 13, the continuous sine wave is applied for 5 s. Because the response is very stable using infinite boundary elements, the response is shown only from 4.8 to 5 s. It is found that the ratio of *I*/*M* has no influence on the response. The dynamic response obtained from models with different model region sizes are shown in Figs. 13(a and b). Because the infinite boundary element cannot provide the perfect absorption when the incident wave is not perpendicular to the boundary, less energy arrives at the boundaries, and less energy is reflected. When the model region size increased from 5 × 5 m to 10 × 10 m, the distance from the loading point to the boundary increases and the energy that reaches the boundaries is therefore reduced due to the geometric damping. As the model region size increases, the reflection from the boundaries is therefore reduced.

Influence of Region Size

In addition to the infinite boundary, another alternative, the viscoelastic boundary, is also tested for various model region sizes. The point load is applied on the surface at the center of the model. The responses are recorded 0.5 m away from the loading point. The springs and dampers are applied on each boundary node for both the normal and tangential directions. These two different boundaries are compared under the impulse load of 3 cycles of the 4.77-Hz sine wave, as shown in Fig. 14 and a continuous 30-Hz harmonic sine wave, as shown in Fig. 15.

As shown in Fig. 14, when the model is subjected to low-frequency impulse load, two models with different absorbing boundary converges with increasing region size. When the model size gets larger, the model behaves stiffer if the infinite boundary is used, and the model behaves less stiff if the viscoelastic boundary is used. However, this trend is not always followed. As shown in Fig. 15, when the model is subject to a higher frequency, i.e. 30-Hz harmonic load, the response of the model using infinite boundary does not alter a lot by the model size, but the response of the model using viscoelastic boundary vary with model size. The stiffness imposes by the boundary is the major difference between these two boundaries. For the 50 m × 50 m region size, the difference of responses between these different boundaries is negligible. Based on the convergence test, the minimum model region size of 50 × 50 m is required for the given conditions, so the reflection resulting from the part of waves with an incident angle not equals to 0 can be neglected.

Comparison between Viscoelastic Boundary and Infinite Element

Based on the simulation results, the response from both the viscoelastic boundary and the infinite element converged with adequately large model size. In this section, the model size is set as 50 × 50 m

J. Eng. Mech., 2021, 147(2): 04020150

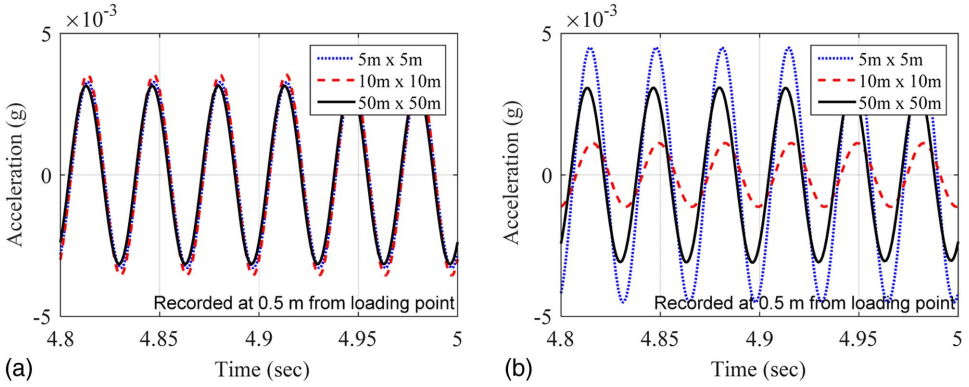

Fig. 15. Dynamic response under 30-Hz continuous excitation: (a) infinite boundary; and (b) viscoelastic boundary.

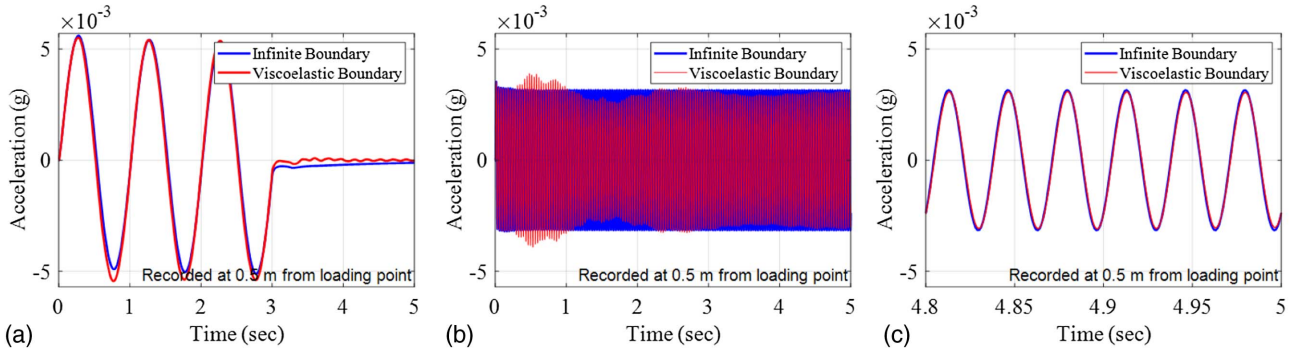

Fig. 16. Dynamic response of the 50 × 50 m FE model: (a) 4.77-Hz impulse; (b) 30-Hz continuous; and (c) 30-Hz continuous (4.8–5 s).

to further investigate the difference between using the viscoelastic boundary and the infinite boundary element.

Fig. 16(a) shows the response when the model is subjected to low-frequency impulse load (4.77 Hz). The response from both boundaries did not show a noticeable reflection effect when the load was paused at 3 s. Under the low-frequency impulse load, the response from the viscoelastic boundary reduces to 0 quicker than the infinite boundary, indicating the viscoelastic boundary is more favorable for impulse excitation. However, when the model is subjected to a continuous 30-Hz harmonic wave, the response from the viscoelastic boundary is not as stable as the simulation result of the infinite boundary. After 4 s, the response from the viscoelastic boundary eventually becomes stable and converges with the response from the infinite boundary is observed after 4 s, as shown in Fig. 16(b). Fig. 16(c) shows the result of 30-Hz continuous excitation from 4.8 to 5 s. As shown in Fig. 16(c), the difference between the simulation results of two boundary conditions are almost negligible after 4.8 s of excitation. Therefore, when the harmonic wave was applied to simulate the periodic barriers in soil, the author recommends conducting parametric analysis to ensure the simulation result obtained from the viscoelastic boundary converges to that of the infinite element.

Analysis Methods

Two analysis methods are used in this study. One is termed a fix-frequency harmonic analysis, and the other is a time-history analysis. The differences between these two analysis methods are their loading protocol and the way to process data.

Fig. 17 is the schematic drawing of the FE model with the one unit of periodic barrier and its surrounding soil. Two different absorbing boundaries, the infinite boundary and viscoelastic boundary, are used to minimize the reflection from the model boundary. The excitation is applied at the surface near the center of the model. The loading distance is defined by the distance between the vibration source and the edge of the periodic barrier.

In this section, the model region size is set as 150 × 150 m, which is adequate to avoid notable reflection from the boundary based on the results presented previously. Besides, the requirements for element type and maximum mesh size for modeling periodic barriers are also selected. When the excitation is applied vertically, the energy is carried mostly by the Rayleigh wave on the surface; when the excitation is applied horizontally, the energy is carried mostly by P wave on the surface. Fig. 18 shows the screening performance in terms of FRF when the excitation is applied on the surface in the vertical direction. Fig. 19 shows the results when the excitation is applied in the horizontal direction. For the fix-frequency harmonic analysis, the continuous harmonic sine wave ranging from 15 to 100 Hz were studied. For the time-history analysis, the El Centro earthquake and the San Fernando earthquake were adopted to investigate the influence of seismic excitation on the simulation results. Both time-history records are obtained from the PEER ground motion database. Because the frequency range of interest in this study is 15–100 Hz, the time axis of both time-history records is scaled by multiplying with scale factors so that its main frequency content is also within 15 and 100 Hz. In this study, the scale factors are 0.025 and 0.05 for El Centro and San Fernando, respectively. When the excitation was applied right on

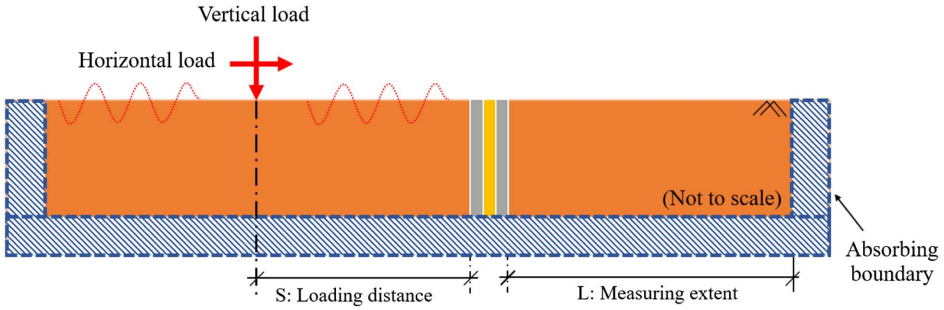

Fig. 17. Schematic drawing of modeling the periodic barrier.

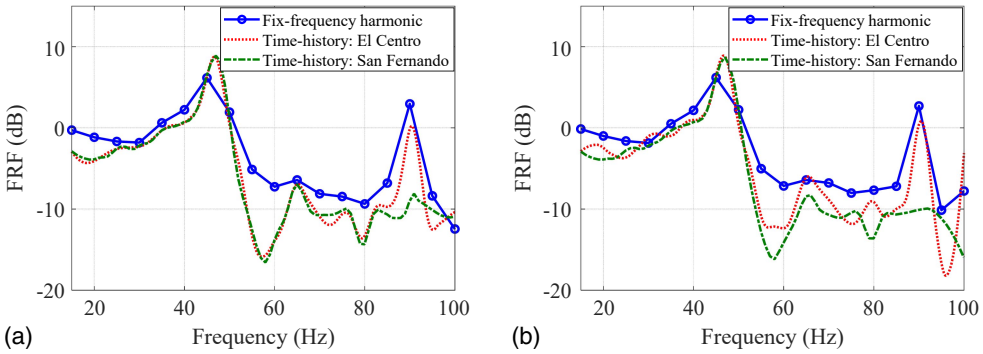

Fig. 18. *FRF* of one unit periodic barrier under vertical excitation on barrier edge: (a) infinite boundary; and (b) viscoelastic boundary.

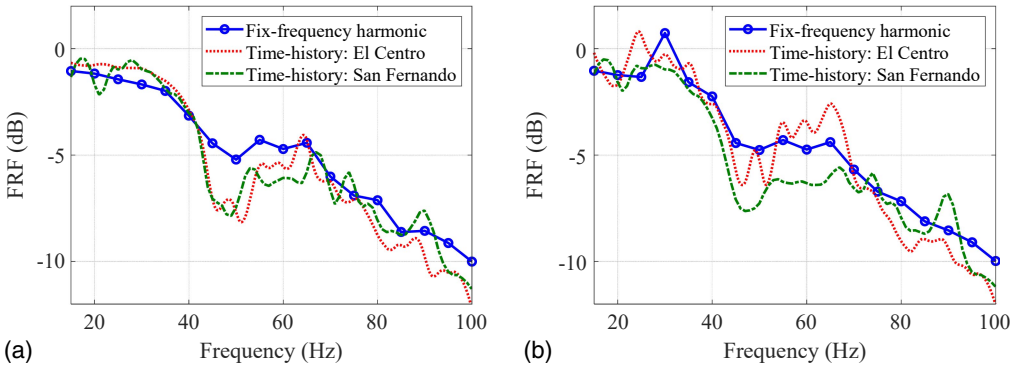

Fig. 19. *FRF* of one unit periodic barrier under horizontal excitation applied on the edge of the barrier: (a) infinite boundary; and (b) viscoelastic boundary.

the edge of the periodic barrier, which means its loading distance equals 0. The results from fix-frequency harmonic analysis and time-history analysis are compared in Figs. 18 and 19.

Based on the definition of the *FRF*, negative *FRF* indicates the attenuation, and positive *FRF* indicates the amplification. Figs. 18 and 19 show the performance of one unit periodic barrier under vertical excitation and horizontal excitation, respectively. It is found different types of absorbing boundaries, infinite boundary, and viscoelastic boundary yield almost identical results. The results obtained from two analysis methods, the fix-frequency harmonic analysis and time-history analysis, have a very strong correlation. Even though the value is not identical, the overall trend is captured. By using time-history analysis, the computing time can be significantly reduced and still maintain acceptable accuracy. Based on the simulation results in this section, it is recommended to use time history analysis to investigate the performance of the periodic barrier.

Figs. 18 and 19 show the fact that even though the soil response behind the periodic barrier is expected to be smaller compared to the free field excitation, it is found that the response reduction due to the periodic barrier not only depends on the exciting frequency but also depends on the excitation direction.

Number of Barriers

This section further investigates the effect of number barriers on the *FRF*. An additional number of unit cells of the periodic barrier is added, where the second unit cell is placed 3.048 m (10 ft) apart

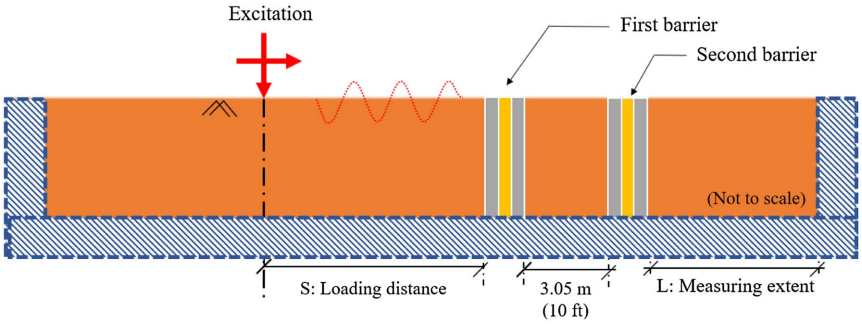

Fig. 20. Schematic drawing for the isolating system with two units of periodic barriers.

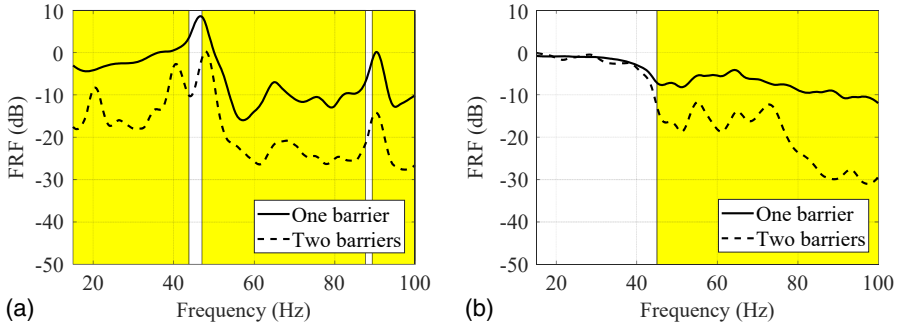

Fig. 21. Effect of the number of barriers on the performance of the periodic barriers: (a) vertical excitation; and (b) horizontal excitation.

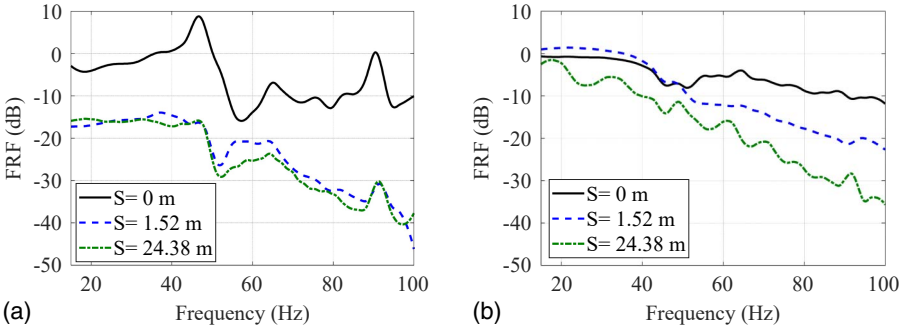

Fig. 22. Effect of loading distance on FRF of one unit periodic barrier: (a) vertical excitation; and (b) horizontal excitation.

from the first unit cell, as shown in schematic drawing Fig. 20. When the excitation is applied on the edge of the first unit of periodic barrier in either vertical or horizontal direction, the loading distance, S, equals to 0. By comparing the soil response when there are barriers and when there is no barrier, the FRF is calculated within the measuring extent starting from behind the barriers.

Fig. 21 shows the performance of one or two periodic barriers under vertical and horizontal excitation. The theoretical frequency band gaps of the periodic barrier for Rayleigh wave and P wave are highlighted with the yellow patches along with the FRF results in Figs. 21(a and b), respectively. A negative FRF value indicates the attenuation induced by the existence of the barrier, the lower the FRF value, the more attenuation is observed. It is found the attenuation is observed in theoretical frequency band gaps. The performance of the periodic barrier improves as the second barrier is added to the isolation system. The improvement is particularly conspicuous within the frequency regions that coincide with the theoretical frequency band gaps. The improvement made by adding the second barrier is less within the frequency range of the theoretical pass band especially when the model is subject to horizontal excitation.

Loading Distance

Loading distance is defined by the distance between the vibration source to the edge of the barrier. This section aims to investigate the effect of loading distance on the FRF. In addition to the case when the excitation is applied on the edge of the periodic barrier, two other loading distances 1.52 and 24.38 m, are selected for the load to be placed on. The excitation is applied in either vertical or horizontal direction. Fig. 22 presents the performance of a unit of the periodic barrier when the excitation is applied at various loading

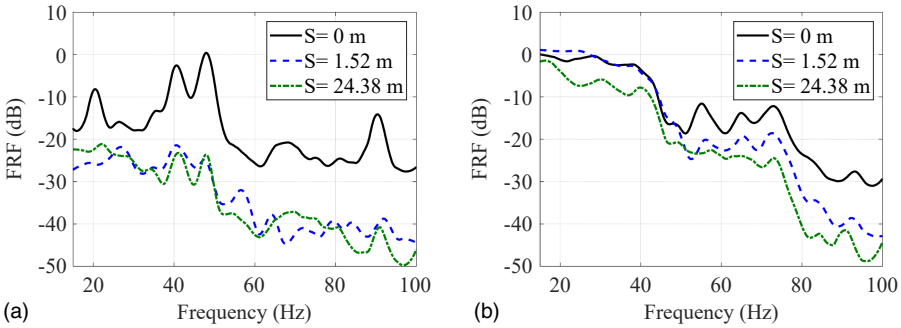

Fig. 23. Effect of loading distance on *FRF* of two periodic barriers: (a) vertical excitation; and (b) horizontal excitation.

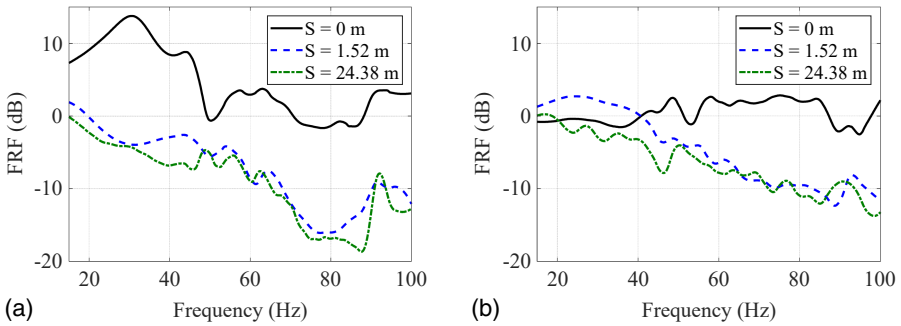

Fig. 24. *FRF* of one unit periodic barrier with the barrier depth of 1.52 m: (a) vertical excitation; and (b) horizontal excitation.

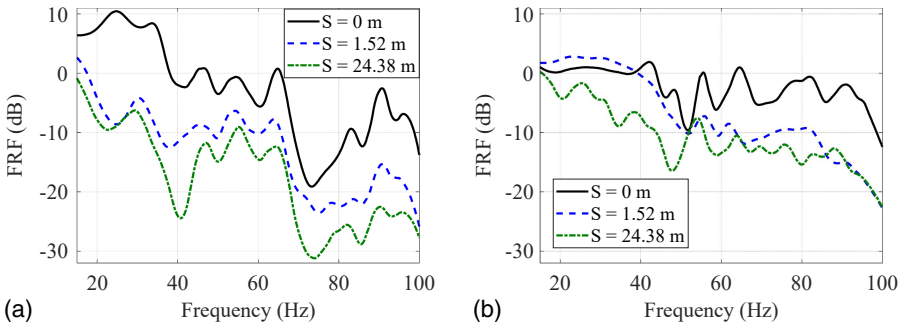

Fig. 25. *FRF* of two periodic barriers with the barrier depth of 1.52 m: (a) vertical excitation; and (b) horizontal excitation.

distances. Fig. 23 presents the performance of two units of periodic barriers when the excitation is placed at various loading distance.

As shown in Figs. 22 and 23, when the loading distance increases from 0 to 1.52 m, the performance of the periodic barriers is greatly enhanced. However, when the loading distance increases from 1.52 to 24.38 m, the performance of the periodic barriers does not improve as much. This shows that even though the periodic barrier is more effective in isolating the vibration from a farther distance when loading distance is more than 1.52 m, the geometric decay of the energy in the soil is the dominant factor in reducing the response rather than the filtering mechanism of the barrier. Moreover, by comparing Figs. 22 and 23, the performance of the periodic barriers is better when there are two periodic barriers than when there is one periodic barrier.

Barrier Depth

This section aims to discuss the effect of the barrier depth on the screening effectiveness of the periodic barriers. The depth of the barrier is considered the most important parameter that can affect the performance of the barrier. Figs. 24 and 25 show the performance of the periodic barrier when the barrier depth is reduced to 1.52 m (5 ft).

Comparing Figs. 22 and 24 or Figs. 23 and 25, the periodic barrier with infinite depth is more effective in screening the vibration behind the barrier than the periodic barrier with 1.52 m depth. The most distinct result found in Figs. 22 and 24 is that when the excitation is applied on the edge of the periodic barrier (S = 0), the amplification is only found outside the frequency band gaps in Fig. 22, but the *FRF*s are all above zero in Fig. 24, which suggests

the response amplification occurs within the whole frequency range of interest (15–100 Hz). This observation conflicts with a common conclusion that either the soft or stiff barrier should be effective when the barrier depth reaches 0.6 times the Rayleigh wavelength of the soil (Al-Hussaini and Ahmad 1991; Alzawi and El Naggar 2011; Coulier et al. 2015; Persson et al. 2016; Saikia 2014; Thompson et al. 2016). Because the barrier depth is fixed to 1.52 m in this section, the barrier depth is larger than 0.6 times the Rayleigh wavelength when the exciting frequency excesses 72 Hz with the given soil conditions. As shown in Figs. 24 and 25, when the loading distance equals 1.52 or 24.38 m, the results agree with this conclusion regardless of the excitation direction, whereas when the loading distance equals to zero, the response reduction is not observed as expected for frequency above 72 Hz. This is because there is no enough room for the wave to attenuate along the depth direction as the excitation is applied directly on the edge of the periodic barrier.

As shown in Figs. 24 and 25, by increasing the loading distance and number of barriers, the barriers show better performance when it is subjected to either vertical or horizontal excitation. Moreover, it was found that shorter depth is required to achieve the same amount of response reduction when dual barriers are used (Saikia 2014). As shown in Fig. 25, the *FRF*s are below 0 as the barrier depth reaches 0.3 times the Rayleigh wavelength (40 Hz above) when dual barriers are used. The reason is that there is enough space between the two units of barriers for waves to attenuate along the depth direction in the soil.

Conclusions

The theoretical frequency band gap with the given properties of the periodic barrier is first solved by the transfer matrix method. After determining the model size, mesh size, and element type from the convergence analysis. 2D FE simulation is used to investigate the performance of the barrier adapting the periodic metamaterial by comparing the responses when there is a barrier with the response when there is no barrier at points behind the designated protected area. Based on the FE simulation results, the following conclusions can be drawn:

1. Other than the fix-frequency harmonic analysis, the time-history analysis is adopted to boost computing efficiency. The results from the two analysis methods are showing a good agreement with each other;
2. After testing the mesh size, element type, and analysis methods, the FE simulation is validated with the shake table test on the 1D periodic foundation. The element type, mesh size, and analysis method used in the FE simulation are proved to be capable of reproducing the results from the experiment;
3. The loading distance and the number of the periodic barrier are investigated. It is found the periodic barrier is more effective as the loading distance increases, and adding the number of periodic barriers can improve its screening effectiveness in theoretical frequency band gaps;
4. The *FRF* results comply with the theoretical frequency band gaps when the loading is directly applied on the edge of the periodic barrier with infinite depth. As the loading distance increases, even though the screening effectiveness improves, the attenuation zone cannot be identified easily due to the inclusion of the soil. When the loading distance increases, the soil becomes one part of the metamaterial, which leads to different theoretical band gaps. Therefore, adding a layer of soil can widen the theoretical frequency band gap. However, as the loading distance further increases from 1.52 to 24.38 m, the improvement contributed by the soil layer is not proportion to the improvement from 0 to 1.52 m. The *FRF* results are relatively close to each other for the case of loading distance equals to 1.52 and 24.38 m, which means the effect of loading distance is not much when the loading distance is more than 1.52 m; and
5. With the barrier depth reduced to 1.52 m, the periodic barrier is less effective in screening the vibration than the barrier with infinite depth. Response amplification is observed when the excitation is applied exactly on the edge of the periodic barrier because there is no space between the vibration source and the barrier for waves to attenuate along the depth direction. Therefore, the periodic barrier with 1.52 m depth is found to have better screening effectiveness when increasing the loading distance or number of barriers.

Data Availability Statement

All data, models, or codes that support the findings of this study are available from the corresponding author upon reasonable request.

Acknowledgments

This research is financially supported by the National Science Foundation under Award No. 1761659. The authors acknowledge the use of Opuntia Cluster for the computing works conducted in this paper. The resources were provided by the Core Facility for Advanced Computing and Data Science at the University of Houston.

References

Al-Hussaini, T. M., and S. Ahmad. 1991. "Design of wave barriers for reduction of horizontal ground vibration." *J. Geotech. Eng.* 117 (4): 616–636. https://doi.org/10.1061/(ASCE)0733-9410(1992)118:8(1282.2).

Alzawi, A., and M. H. El Naggar. 2011. "Full scale experimental study on vibration scattering using open and in-filled (GeoFoam) wave barriers." *Soil Dyn. Earthquake Eng.* 31 (3): 306–317. https://doi.org/10.1016/j.soildyn.2010.08.010.

Andersen, L., and S. R. Nielsen. 2005. "Reduction of ground vibration by means of barriers or soil improvement along a railway track." *Soil Dyn. Earthquake Eng.* 25 (7–10): 701–716. https://doi.org/10.1016/j.soildyn.2005.04.007.

Bao, J., Z. Shi, and H. Xiang. 2011. "Dynamic responses of a structure with periodic foundations." *J. Eng. Mech.* 138 (7): 761–769. https://doi.org/10.1061/(ASCE)EM.1943-7889.0000383.

Beskos, D., B. Dasgupta, and I. Vardoulakis. 1986. "Vibration isolation using open or filled trenches." *Comput. Mech.* 1 (1): 43–63. https://doi.org/10.1007/BF00298637.

Çelebi, E., S. Fırat, G. Beyhan, İ. Çankaya, İ. Vural, and O. Kırtel. 2009. "Field experiments on wave propagation and vibration isolation by using wave barriers." *Soil Dyn. Earthquake Eng.* 29 (5): 824–833. https://doi.org/10.1016/j.soildyn.2008.08.007.

Cheng, Z., and Z. Shi. 2013. "Novel composite periodic structures with attenuation zones." *Eng. Struct.* 56 (Nov): 1271–1282. https://doi.org/10.1016/j.engstruct.2013.07.003.

Coulier, P., V. Cuéllar, G. Degrande, and G. Lombaert. 2015. "Experimental and numerical evaluation of the effectiveness of a stiff wave barrier in the soil." *Soil Dyn. Earthquake Eng.* 77 (Oct): 238–253. https://doi.org/10.1016/j.soildyn.2015.04.007.

Ekanayake, S. D., D. Liyanapathirana, and C. J. Leo. 2014. "Attenuation of ground vibrations using in-filled wave barriers." *Soil Dyn. Earthquake Eng.* 67 (Dec): 290–300. https://doi.org/10.1016/j.soildyn.2014.10.004.

Gao, G., N. Li, and X. Gu. 2015. "Field experiment and numerical study on active vibration isolation by horizontal blocks in layered ground under

vertical loading." *Soil Dyn. Earthquake Eng.* 69 (Feb): 251–261. https://doi.org/10.1016/j.soildyn.2014.11.006.
Gao, G., Z. Li, C. Qiu, and Z. Yue. 2006. "Three-dimensional analysis of rows of piles as passive barriers for ground vibration isolation." *Soil Dyn. Earthquake Eng.* 26 (11): 1015–1027. https://doi.org/10.1016/j.soildyn.2006.02.005.
Huang, J., and Z. Shi. 2013. "Attenuation zones of periodic pile barriers and its application in vibration reduction for plane waves." *J. Sound Vib.* 332 (19): 4423–4439. https://doi.org/10.1016/j.jsv.2013.03.028.
Huang, J. K., W. Liu, and Z. F. Shi. 2017. "Surface-wave attenuation zone of layered periodic structures and feasible application in ground vibration reduction." *Constr. Build. Mater.* 141 (Jun): 1–11. https://doi.org/10.1016/j.conbuildmat.2017.02.153.
Jia, G., and Z. Shi. 2010. "A new seismic isolation system and its feasibility study." *Earthquake Eng. Eng. Vibr.* 9 (1): 75–82. https://doi.org/10.1007/s11803-010-8159-8.
Kattis, S., D. Polyzos, and D. Beskos. 1999. "Vibration isolation by a row of piles using a 3-D frequency domain BEM." *Int. J. Numer. Methods Eng.* 46 (5): 713–728. https://doi.org/10.1002/(SICI)1097-0207(19991020)46:5<713::AID-NME693>3.0.CO;2-U.
Leung, K., D. Beskos, and I. Vardoulakis. 1990. "Vibration isolation using open or filled trenches." *Comput. Mech.* 7 (2): 137–148. https://doi.org/10.1007/BF00375927.
Liao, S., and D. A. Sangrey. 1978. "Use of piles as isolation barriers." *J. Geotech. Geoenviron. Eng.* 104 (9): 1139–1152.
Liu, X. N., Z. F. Shi, H. J. Xiang, and Y. L. Mo. 2015. "Attenuation zones of periodic pile barriers with initial stress." *Soil Dyn. Earthquake Eng.* 77 (Oct): 381–390. https://doi.org/10.1016/j.soildyn.2015.06.010.
Persson, P., K. Persson, and G. Sandberg. 2016. "Numerical study of reduction in ground vibrations by using barriers." *Eng. Struct.* 115 (May): 18–27. https://doi.org/10.1016/j.engstruct.2016.02.025.
Pu, X., and Z. Shi. 2019. "Periodic pile barriers for Rayleigh wave isolation in a poroelastic half-space." *Soil Dyn. Earthquake Eng.* 121 (Jun): 75–86. https://doi.org/10.1016/j.soildyn.2019.02.029.
Qiu, B. 2014. "Numerical study on vibration isolation by wave barrier and protection of existing tunnel under explosions." Ph.D. thesis, Laboratory of Civil and Environmental Engineering, Institut National des Sciences Appliquées de Lyon.
Saikia, A. 2014. "Numerical study on screening of surface waves using a pair of softer backfilled trenches." *Soil Dyn. Earthquake Eng.* 65 (Oct): 206–213. https://doi.org/10.1016/j.soildyn.2014.05.012.
Segol, G., J. F. Abel, and P. C. Lee. 1978. "Amplitude reduction of surface waves by trenches." *J. Eng. Mech. Div.* 104 (3): 621–641.
Shi, Z., Z. Cheng, and H. Xiang. 2017. *Periodic structure: Theory and applications to seismic isolation and vibration reduction*. [In Chinese.] Beijing: Science Press.
Smith, M. 2016. *ABAQUS/standard user's manual, version 2017*. Providence, RI: Simulia.
Thompson, D., J. Jiang, M. Toward, M. Hussein, E. Ntotsios, A. Dijckmans, P. Coulier, G. Lombaert, and G. Degrande. 2016. "Reducing railway-induced ground-borne vibration by using open trenches and soft-filled barriers." *Soil Dyn. Earthquake Eng.* 88 (Sep): 45–59. https://doi.org/10.1016/j.soildyn.2016.05.009.
Waas, G. 1972. "Linear two-dimensional analysis of soil dynamics problems in semi-infinite layer media." Ph.D. thesis, Dept. of Civil and Environmental Engineering, Univ. of California, Berkeley.
Wang, J.-G., W. Sun, and S. Anand. 2009. "Numerical investigation on active isolation of ground shock by soft porous layers." *J. Sound Vib.* 321 (3–5): 492–509. https://doi.org/10.1016/j.jsv.2008.09.047.
Witarto, W., S. Wang, C. Yang, X. Nie, Y. L. Mo, K. Chang, Y. Tang, and R. Kassawara. 2018. "Seismic isolation of small modular reactors using metamaterials." *AIP Adv.* 8 (4): 045307. https://doi.org/10.1063/1.5020161.
Witarto, W., S. Wang, C. Yang, J. Wang, Y. L. Mo, K. Chang, and Y. Tang. 2019. "Three-dimensional periodic materials as seismic base isolator for nuclear infrastructure." *AIP Adv.* 9 (4): 045014. https://doi.org/10.1063/1.5088609.
Woods, R. D. 1968. "Screening of surface waves in soils. Ph.D. thesis, Industry Program of the College of Engineering, The Univ. of Michigan.
Xiang, H., Z. Shi, S. Wang, and Y. L. Mo. 2012. "Periodic materials-based vibration attenuation in layered foundations: Experimental validation." *Smart Mater. Struct.* 21 (11): 112003. https://doi.org/10.1088/0964-1726/21/11/112003.
Yan, Y., Z. Cheng, F. Menq, Y. L. Mo, Y. Tang, and Z. Shi. 2015. "Three dimensional periodic foundations for base seismic isolation." *Smart Mater. Struct.* 24 (7): 075006. https://doi.org/10.1088/0964-1726/24/7/075006.
Yan, Y., A. Laskar, Z. Cheng, F. Menq, Y. Tang, Y. L. Mo, and Z. Shi. 2014a. "Seismic isolation of two dimensional periodic foundations." *J. Appl. Phys.* 116 (4): 044908. https://doi.org/10.1063/1.4891837.
Yan, Y., Y.-L. Mo, F.-Y. Menq, I. Stokoe, H. Kenneth, J. Perkins, and Y. Tang. 2014b. *Development of seismic isolation systems using periodic materials*. Idaho Falls, ID: Battelle Energy Alliance.